Engineering Science and Technology, an International Journal 20 (2017) 1450–1459

HOSTED BY

Contents lists available at ScienceDirect

Engineering Science and Technology, an International Journal

journal homepage: www.elsevier.com/locate/jestch

Full Length Article

Enhanced method of rotor speed and position estimation of permanent magnet synchronous Machine based on stator SRF-PLL

R. Vijayapriya, P. Raja *, M.P. Selvan

Department of Electrical and Electronics Engineering, National Institute of Technology, Tiruchirappalli 620 015, Tamil Nadu, India

ARTICLE INFO

Article history:
Received 15 June 2017
Revised 28 August 2017
Accepted 21 September 2017
Available online 27 October 2017

Keywords:
Low pass filter
Synchronous reference frame
Phase locked loop
PMSM
Stator flux
Speed and position estimation

ABSTRACT

A stator flux oriented synchronous reference frame - phase locked loop (SRF-PLL) is proposed for the precise computation of rotor speed and position of permanent magnet synchronous machine (PMSM). A direct method of rotational speed computation based on the stator electromotive force (EMF) is initially formulated. Using the speed as a reference to the inverse Park and Clarke transformation blocks, the three-phase positive sequence stator flux is derived. A pre-stage low pass filter (LPF) is implemented to cancel out the ripples in the d-q components of the stator flux introduced by the dynamic operating conditions of inverter non-linearities and grid disturbances. The estimated three-phase positive sequence stator flux is used to compute the rotor position by aligning the total stator flux along the direct axis through a PLL block. Provision of the frequency amendment and ripple cancellation outside the PLL block results in a fast-dynamic response with an enhanced frequency adaptable capability. To validate the effectiveness of the proposed method, the sensorless vector control of grid integrated PMSM based wind-driven generator (WG) is analytically verified using the PSCAD/EMTDC simulation tool under various dynamic operating conditions such as wind speed variation and grid disturbances.

1. Introduction

Permanent magnet synchronous machines (PMSMs) are making remarkable advancement in the field of various application specific drives due to the development of high performance magnetic material adjuvant to higher torque density and efficiency [1–3]. Specifically, in wind mill generators, its development has attracted a great deal for the inherent characteristics of high-controllability, robustness and maintenance-free operation [4–6]. In such ac drive applications, vector control has gained popularity owing to high-performance torque control characteristics like that of dc machines. Conventionally, the controllers employed involves in sensing the rotor speed and position using a rotary encoder. However, such hard-wired sensors with increased cost, reduced reliability and wired feedback demands a sensorless estimation of rotor speed and position. [7–9]. An accurate estimation of rotor speed and position appears to be more challenging under dynamic operating conditions like wind speed variation and grid disturbances in the grid integrated wind-driven generators (WGs). Several open-loop and closed-loop schemes of sensorless rotor speed/position estimation are reviewed in [10], where the precise estimation of the rotor speed/position by means of the open-loop scheme strongly depends on the accurate measurement of system parameters.

Rotor speed estimation is generally carried out by differentiating the rotor position which is computed by arc tangent of orthogonal electromotive force (EMF) or the stator flux. Adaptive mechanisms such as sliding mode observer (SMO) and model reference adaptive system (MRAS) have been explored to estimate the stator EMF or flux by comparing the PMSM parameters with the reference model values. The observer models in [11,12] are repeatedly tuned to match the estimated system values to the actual values based on fuzzy training and artificial neural network, respectively. Likewise, a traditional observer [13], an iterative SMO [14], SMO with sigmoid function [15] and a discrete time-SMO with parameter adaption scheme [16] have been implemented to estimate the EMF. A direct method of stator flux estimation from the measured stator current and commanded stator voltage is also presented in [17,18]. In the available direct and indirect methods, apart from complex computational procedures, rotor speed estimation results in transient errors caused by a low pass filter (LPF) employed to suppress the spikes introduced during differential operation of rotor position.

* Corresponding author.
E-mail addresses: vijayapriiyaa@yahoo.co.in (R. Vijayapriya), praja@nitt.edu (P. Raja), selvanmp@nitt.edu (M.P. Selvan).
Peer review under responsibility of Karabuk University.

https://doi.org/10.1016/j.jestch.2017.09.004
2215-0986/

A quasi SMO current model is designed to estimate the stator flux and rotor position with saturation function instead of a sign switching function to mitigate the chattering problem [19]. However, both the non-linear sign and saturation switching functions introduce noise at the estimated system values. To avoid an incorrect parameter convergence of two unknown quantities, the flux linkage and the rotor speed estimation based on extended kalman filter (EKF) and MRAS respectively is proposed in [20]. A similar case is discussed in [21–23] with improved SMO and MRAS method of EMF and rotor speed estimation respectively. A reactive power based MRAS speed estimation was discussed in [24]. However, the reference models use an adaptive filter at the output stage to filter out the noisy contents from the estimated system quantities (EMF or flux), which adversely affects the dynamic speed tracking ability of the models. Generally, rotor position estimation of these conventional methods result in error amplification because of an arc tangent computation of estimated orthogonal back-EMFs.

A quadrature-phase locked loop (Q-PLL) based rotor position computation by applying the estimated stationary frame of back EMF is described in [25–27]. On the contrary, in [28–30] rotor speed and position are computed by forcing the position error to zero through the controller. The position error is estimated by tracking the difference between the real d-q axis and the estimated/observed axis. Instead of forcing the position error to be zero, a voltage pulse is applied on one of the estimated axis and a coupling component is observed on the other axis. The existence of the coupling component indicates the position error and the component is processed through the controller to obtain zero position error [31]. Regardless of PLL and estimated d-q axis formation of rotor position computation, the speed/d-q frame quantities are predicted on model based techniques. Since adaptive models are framed with reduced order computation under several assumptions and approximations, rotor speed will not be precisely estimated in addition to complex computational procedures.

The objective of the present study is to bring forth a simple and accurate rotor speed/position computation without adopting observer based models for the enhanced control of grid integrated PMSM based WG under various dynamic operating conditions. A stator flux oriented synchronous reference frame (SRF) PLL with a pre-stage LPF and frequency amendment is proposed in this paper to precisely compute the rotor speed and position. Section 2 describes the analytical modelling of the wind turbine coupled PMSM. Section 3 illustrates the dynamic operational impacts on the system parameters of WG integrated to the grid by means of a back to back voltage source converters (VSCs). Section 4 details the proposed method of rotor speed and position computation. This section also demonstrates the controlling techniques adopted for the back to back converters. Section 5 presents the analytical simulation of the proposed sensorless computation of the rotor speed and position for the grid integrated PMSM based WG under various dynamic operating conditions using the PSCAD/EMTDC simulation tool. Section 6 concludes the validation of the proposed method.

2. PMSG modelling

The PMSM modelling in stationary reference frame [32] can be expressed as

$$v_{s\alpha} = \frac{d\psi_{s\alpha}}{dt} + R_s i_{s\alpha} \tag{1}$$

$$v_{s\beta} = \frac{d\psi_{s\beta}}{dt} + R_s i_{s\beta} \tag{2}$$

Also, according to the permanent magnet (PM) rotor flux orientation, the machine modelling in synchronous reference frame can be described as

$$v_{sd} = -\omega_{es}\psi_{sq} + R_s i_{sd} + \frac{d\psi_{sd}}{dt} \tag{3}$$

$$v_{sq} = \omega_{es}\psi_{sd} + R_s i_{sq} + \frac{d\psi_{sq}}{dt} \tag{4}$$

where the stator flux linkage in the d-q frame is expressed as summation of the induced flux in the stator due the stator current and the rotor PM flux

$$\psi_{sd} = L_{sd} i_{sd} + \psi_{rd} \tag{5}$$

$$\psi_{sq} = L_{sq} i_{sq} + \psi_{rq} \tag{6}$$

The rotor magnets are assumed to be aligned along d-axis, therefore q-axis magnetic flux is zero and the rotor fluxes can be represented as

$$\psi_{rd} = \psi_{PM} \tag{7}$$

$$\psi_{rq} = 0 \tag{8}$$

The two-mass drive train shaft model of the PMSM is employed as given in (9)–(11) for an accurate depiction of the system mechanical characteristics [33]

$$T_{wt} - T_{sh} = J_{wt}\frac{d\omega_{wt}}{dt} \tag{9}$$

$$T_{sh} - T_e = J_r\frac{d\omega_r}{dt} \tag{10}$$

$$T_{sh} = K(\omega_{wt} - \omega_r) \tag{11}$$

where the shaft stiffness K is inversely proportional to number of pole pairs.

3. Characterization of grid disturbances and inverter non-linearity

Rotor position can be computed from the stator flux, as the stator and rotor flux vectors rotate synchronously. The precise estimation of rotor speed and position is possible only if an undistorted SRF component process through the PLL block. However, grid disturbances and inverter non-linearities introduces ripple in the SRF components. Hence, to estimate the rotor speed and position precisely under different dynamic operating conditions of the system, the impact on the generator parameters must be primarily analysed quantitatively.

Various grid disturbances such as unsymmetrical voltage sag and swell, phase-jump, dc-offset and harmonics introduce ripples in the dc-link voltage and current which reflects correspondingly in the stator current, EMF and the flux. Since, rotor position estimation relies on the stator flux information, most importantly the frequency of ripples in the stator flux need to be computed for each case. To effectively determine the impact of various grid disturbances on system parameters and to implement vector control for the back to back converters, controllers are modelled in synchronous reference frame. The space vector representation of grid modelling by aligning the grid phase voltage along q-axis is depicted in Fig. 1. The impact of most frequent grid disturbances that occur at wind power system grid integration point are analysed in the following sub sections [34].

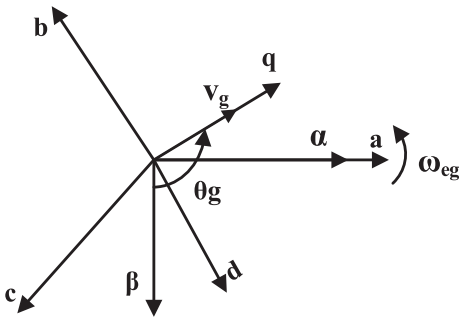

Fig. 1. Space vector representation of grid phase voltage.

3.1. Unsymmetrical voltage sag and phase jump

Considering xV_m of grid phase voltage magnitude and ϕ^o phase - angle jump in 'a-phase', the three-phase grid voltage can be expressed as

$$v_{ga} = xV_m \sin(\theta_g + \phi) \tag{12}$$

$$v_{gb} = V_m \sin\left(\theta_g - \frac{2\pi}{3}\right) \tag{13}$$

$$v_{gc} = V_m \sin\left(\theta_g + \frac{2\pi}{3}\right) \tag{14}$$

By applying Clarke's transformation as per the space vector orientation depicted in Fig. 1, the grid voltages in stationary reference frame can be computed as

$$v_{g\alpha} = \frac{2}{3}xV_m \sin\theta_g \cos\phi + \frac{2}{3}xV_m \cos\theta_g \sin\phi + \frac{1}{3}V_m \sin\theta_g \tag{15}$$

$$v_{g\beta} = V_m \cos\theta_g \tag{16}$$

Under normal grid operation, i.e. for 100% of grid phase voltage magnitude with zero phase – angle jump of $\phi = 0^0$, (15) and (16) can be written as

$$v_{g\alpha} = V_m \sin\theta_g \tag{17}$$

$$v_{g\beta} = V_m \cos\theta_g \tag{18}$$

It is clear from (15) and (16) that, the stationary reference frame voltages are not equal in magnitude under voltage sag and phase-jump and their magnitude varies in proportion to the dip and phase-angle jump of the grid voltage. This effect exactly replicates in the synchronous d-q frame as oscillation components and the grid voltages in positive synchronous frame can be expressed as

$$v^+_{gddc} = \underbrace{\frac{V_m}{3}\sin 2\theta_g(x-1)}_{osc} \tag{19}$$

$$v^+_{gqdc} = \underbrace{\frac{V_m}{3}(x+2)}_{dc} + \underbrace{\frac{V_m}{3}(1-x)\cos 2\theta_g}_{osc} \tag{20}$$

Accordingly, the synchronous reference frame voltages are not pure dc and it also has double frequency oscillation components under voltage sag and phase jump.

3.2. Voltage harmonics

For grid disturbance with the predominant components of 5th and 7th harmonics the stationary and synchronous reference frame grid voltages can be computed as

$$v_{g\alpha} = V_1 \sin\theta_g + V_5 \sin 5\theta_g + V_7 \sin 7\theta_g \tag{21}$$

$$v_{g\beta} = V_1 \cos\theta_g - V_5 \cos 5\theta_g + V_7 \cos 7\theta_g \tag{22}$$

$$v^+_{gddc} = \underbrace{-V_5 \sin 6\theta_g - V_7 \sin 6\theta_g}_{osc} \tag{23}$$

$$v^+_{gqdc} = \underbrace{V_{1\_dc}}_{} \underbrace{- V_5 \cos 6\theta_g + V_7 \cos 6\theta_g}_{osc} \tag{24}$$

where V_1, V_5 and V_7 represents the fundamental, 5th and 7th harmonic components of the grid voltage. It is noted that the magnitude of $v_{g\alpha}$ and $v_{g\beta}$ are not equal due to the presence of harmonics. This variation in magnitude imitate as oscillation in the d-q frame grid voltages with six times the grid frequency oscillation.

3.3. DC offset

The grid voltages in stationary and SRF with a dc offset of V_{off} in 'a-phase' grid voltage can be expressed as

$$v_{g\alpha} = V_m \sin\theta_g + \frac{2}{3}V_{off} \tag{25}$$

$$v_{g\beta} = V_m \cos\theta_g \tag{26}$$

$$v^+_{gddc} = \underbrace{-\frac{2}{3}V_{off}\cos\theta_g}_{osc} \tag{27}$$

$$v^+_{gqdc} = \underbrace{V_m}_{dc} + \underbrace{\frac{2}{3}V_{off}\sin\theta_g}_{osc} \tag{28}$$

DC offset introduces fundamental frequency oscillation in SRF voltages. In general, the d-q frame grid voltages under various grid disturbances can be expressed as

$$v^+_{gd} = v^+_{gddc} + v^+_{gdosc} \tag{29}$$

$$v^+_{gq} = v^+_{gqdc} + v^+_{gqosc} \tag{30}$$

Consistently the d-q frame grid currents also have a dc and oscillation components and hence the grid active and reactive power. In turn, the variation in active power creates an equivalent oscillation in the dc-link voltage and the currents. Even though PMSM is completely decoupled from the grid by means of a power conditioning circuits, the ripples in the dc-link voltage and current will equally be reflected in the PMSM system parameters under grid disturbances. Henceforth, the stator flux in d-q frame under various grid disturbances can be written as

$$\psi_{sd} = \underbrace{L_{sd}i_{sd+} + \psi_{PM}}_{dc} + \underbrace{L_{sd}i_{sd-}}_{ripple} \tag{31}$$

$$\psi_{sq} = \underbrace{L_{sq}i_{sq+}}_{dc} + \underbrace{L_{sq}i_{sq-}}_{ripple} \tag{32}$$

The presence of ripples in the stator flux makes the rate of change of flux component in (3) and (4) to be a non -zero value and hence this term must be considered for system analysis. The impact of various grid disturbances can be represented in Lissajous pattern of stationary reference frame as illustrated in Fig. 2. Typically, the flux pattern will be circular in shape according to Lissajous curve representation under undistorted stationary reference frame. However, the grid tied WG employing power con-

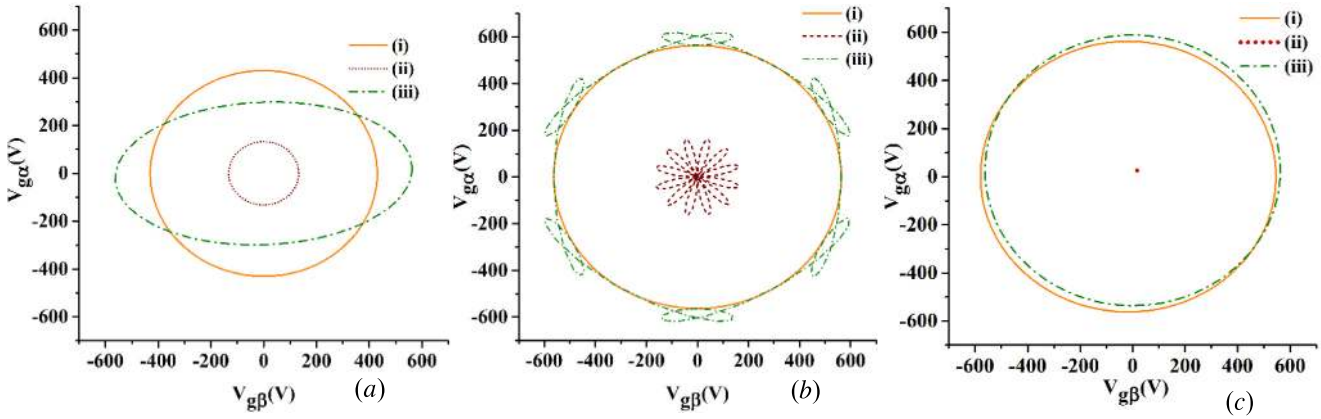

Fig. 2. Lissajous pattern of grid voltage under various grid disturbances [(i) positive sequence, (ii) negative sequence and (iii) resultant] (a) 70% voltage dip and +10° phase-angle jump in "a-phase' (b) 15% of 5th and 7th harmonics (c) 10% of dc voltage offset in 'a-phase'.

verters distort the stator flux due to the existence of various grid disturbances and converter nonlinear characteristics, resulting in non-circular flux pattern.

3.4. Inverter non-linearities

The power conditioning circuit employed for the PMSM also introduces harmonics in the estimated system quantities due to its nonlinear characteristics. Specifically, the voltage source converter causes $(6\theta_r \pm 1)^{th}$ harmonics in the estimated stator flux and result in $(6\theta_r)^{th}$ harmonic ripples in the estimated rotor speed and position [26], analogous to grid voltage harmonics discussed in Section 3.2.

Thus, the influences of various grid disturbances and inverter nonlinearities introduce ripples in d-q axis components of stator flux in addition to dc components resulting in an inaccurate computation of rotor speed and position.

4. Proposed method

The proposed method involves in direct computation of rotor reference angular speed followed by PLL based rotor position estimation without opting any observer/adaptive models.

The procedure for computing the PMSM rotor position comprises of five primary stages. In the first stage, the rotor reference angular frequency is computed while the second stage involves filtering of positive sequence d-q flux components using LPF, third stage transforms the positive sequence d-q fluxes to three-phase components using computed angular frequency in first stage. Then the stator flux position is computed in fourth stage by aligning the total stator flux in assigned d-axis by adopting SRF-PLL. Eventually, in the final stage the rotor position is computed by relating the rotor and assigned stator flux components. The computational process of all the five stages is discussed in detail in the Sections 4.1 and 4.2.

4.1. PMSM reference angular speed computation

The induced EMF of the stator in d-q frames are given by

$$e_{sd} = \omega_{es}\psi_{sq} \tag{33}$$

$$e_{sq} = \omega_{es}\psi_{sd} \tag{34}$$

Rewriting (33) and (34) stator flux components in terms of stator current results in

$$e_{sd} = \omega_{es}L_{sq}i_{sq} \tag{35}$$

$$e_{sq} = \omega_{es}L_{sd}i_{sd} + \psi_{PM}\omega_{es} \tag{36}$$

The induced EMF in the stator can be expressed with q-axis current confined to electromagnetic torque and d-axis current assigned to be zero for controlling purpose

$$e_{sq} = \psi_{PM}\omega_{es} \tag{37}$$

The reference speed ω^*_{es} of the rotor is computed from e_{sq}, which can be determined from (4) based on positive sequence flux component and commanded stator voltage.

4.2. Rotor speed and position computation

The rotor speed and position is computed by assigning the stator flux oriented SRF $d_a - q_a$ as shown in Fig.3a. Primarily, stator flux position δ is computed by forcing q-axis stator flux to be zero in the PLL loop phase detector as depicted in Fig.3b and later the rotor position θ_r is computed based on the relation between the rotor and assigned stator flux components. Effective speed tracking and precise position estimation is possible with PLL only if the loop is updated with angular speed and parameter processed through the loop is ripple free. Accordingly, a speed forward loop with LPF and a loop filter is added in the conventional PLL block in [25,34], respectively. LPF is used to supress the spikes introduced during reference speed manipulation. However, the inclusion of the filters in the PLL block slows down the response and introduces complexity in the controller parameters design. To improve the dynamic response and to exactly track the rotor speed and position a pre-stage LPF and frequency amendment block is proposed in this paper. Initially, a pre-stage LPF is used to extract the positive sequence flux components $\psi^+_{sddc}, \psi^+_{sqdc}$ from the estimated quantities ψ_{sd}, ψ_{sq} and it is transformed into three phase components $\psi^+_{sadc}, \psi^+_{sbdc}, \psi^+_{scdc}$ using the computed reference angular speed. Then the three phase positive sequence fluxes are processed through SRF-PLL to estimate the stator flux position δ by aligning the total stator flux in d_a-axis. Finally, the rotor position is computed by deriving the relation between the rotor and assigned stator flux components as given below

$$\begin{bmatrix}\psi_{rd}\\ \psi_{rq}\end{bmatrix} = \begin{bmatrix}\cos(\delta-\theta_r) - \sin(\delta-\theta_r)\\ \sin(\delta-\theta_r) + \cos(\delta-\theta_r)\end{bmatrix}\begin{bmatrix}\psi_{sd}\\ \psi_{sq}\end{bmatrix} \tag{38}$$

Consistent with rotor flux orientation $(\psi_{rd} = \psi_{PM}, \psi_{rq} = 0)$ and stator flux PLL synchronisation $(\psi_{sd} = \psi_s, \psi_{sq} = 0)$ further simplification of (38) yields

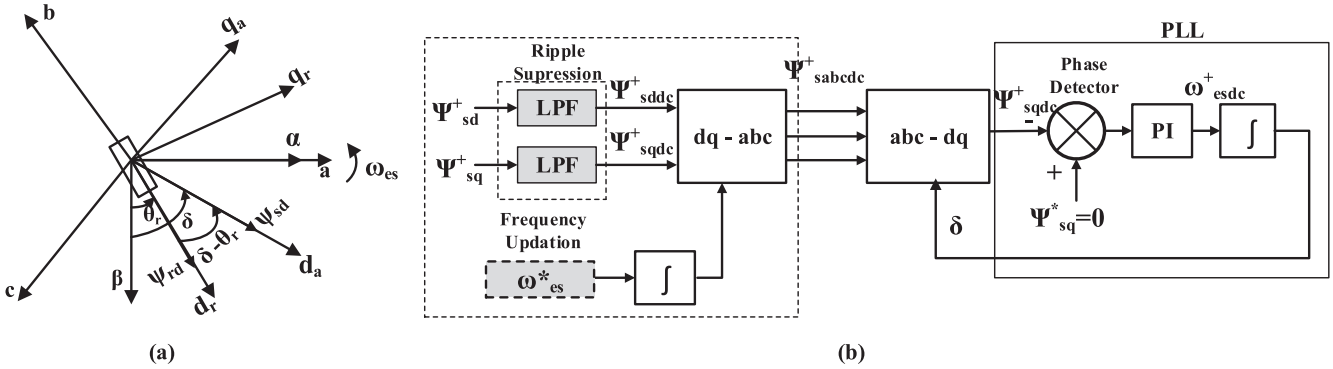

Fig. 3. Proposed method of PMSM rotor speed and position estimation (a) Space vector representation (b) SRF-PLL.

$$\theta_r = \delta - \cos^{-1}\left(\frac{\psi_{PM}}{\psi_s}\right) \tag{39}$$

$$\theta_r = \delta \tag{40}$$

where ψ_s denotes the total stator flux. As θ_r will not be equal to δ, rotor position can be computed using (39). Besides the means of PLL and assigned d-q frame of position estimation, the proposed method does not employ observer models to estimate the system quantities [25–27] or the reference frame [28,29] as depicted in Fig. 4. Moreover, this method gives an optimal solution with fast dynamic response and simple controller design due to filtering and frequency amendment stage outside the PLL block.

This proposed method of sensorless computation of rotor speed and position is employed for the vector control of grid tied PMSM based WG. The control techniques adopted for the back to back VSC is discussed in the subsequent section.

4.3. Vector control of PMSM based WG

An active power regulation of PMSM based WG is realized with dc-link voltage control on machine side converter (MSC) and active power control on grid side converter (GSC) as shown in Fig. 5. The vector control of the MSC is designed with the proposed method of rotor angular speed and position computation. The outer dc-link voltage control loop is formulated using a dc-link current expression

$$C\frac{dV_{dc}}{dt} = i_{dc1} - i_{dc2} = i' \tag{41}$$

From this outer dc-link voltage control loop, the inner loop current reference i^*_{sq} is generated based on the generator electric power

$$P_{em} = 1.5(e_{sq}i_{sq} + e_{sd}i_{sd}) \tag{42}$$

where P_{em} is represented in terms of induced stator emf

GSC is regulated to exercise optimum active power flow in addition to maximum power capturing. Active power control is achieved by regulating the grid active power reference in consonance with the wind power system operating condition [35]. The operating conditions include wind speed variation and grid disturbances. The various grid disturbances considered are symmetrical and unsymmetrical voltage sag, phase-jump, dc-offset, etc. Active power injection during symmetrical voltage sag will not introduce oscillation in the system parameters of dc-link voltage, grid active and reactive power and therefore does not affect the shape of the grid current. Nevertheless, unsymmetrical grid voltage sag, phase jump, harmonics and dc offset introduce considerable percentage of oscillation in the system parameters due to the presence of negative sequence grid voltage component. This results in unsymmetrical and non-sinusoidal grid current injection into the grid. To obtain symmetrical and sinusoidal grid current pattern, a dual vector current control loop has been implemented on the GSC for processing the positive and negative sequence current components [36]. In addition to complex controller design, the technique involves the decomposition of positive and negative sequence components. Whereas in [37], the control scheme has been realized to regulate the positive sequence active and reactive power components to enhance the grid current pattern. Contrast to this method, a control technique is proposed in this paper in positive

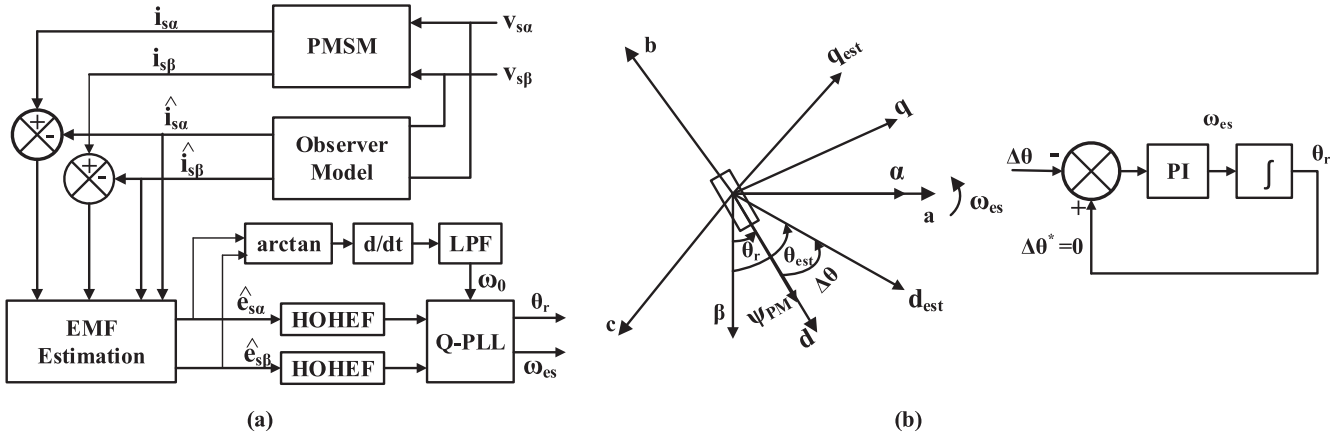

Fig. 4. Conventional methods of PMSM rotor position estimation by (a) Q-PLL (b) estimated d-q frame.

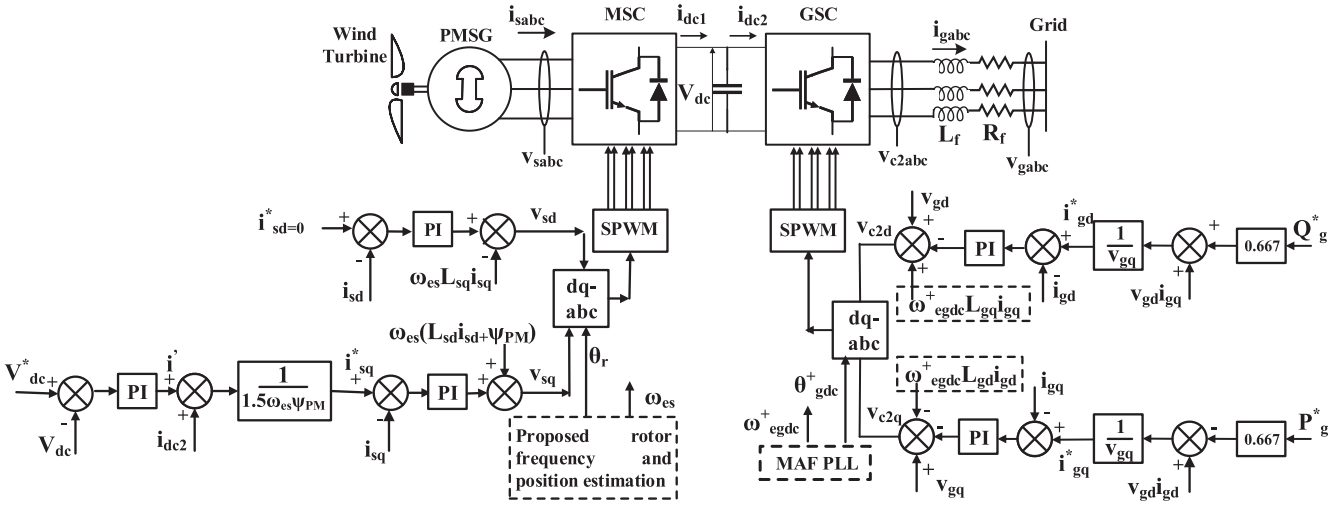

Fig. 5. Sensorless rotor angular frequency and position vector control scheme for PMSM based WG.

synchronous frame with positive sequence components of grid angular frequency and phase angle as depicted in Fig. 5 to obtain the sinusoidal and symmetrical grid current pattern. The grid angular frequency and phase angle are estimated by adopting moving average filter (MAF) based PLL [38].

5. Simulation results

A PSCAD/EMTDC simulation tool is used to design and validate the behavior of the proposed angular speed and position estimator for a 1.5 MW rated PMSM. The method has been analyzed for all possible operating conditions with respect to wind turbine and grid as discussed further.

Case (i) In this case change in wind velocity has been taken as a testing parameter. The speed tracking response of the proposed method for an average change in the wind velocity from 10 m/s to 12 m/s at t = 10 s is illustrated in Fig. 6. It is observed that the estimated rotor angular frequency tracks the actual average value of 267 rad/s and 322 rad/s corresponding to the wind velocity of 10 m/s and 12 m/s respectively. A good tracing of rotational speed is obtained with the worst case transient error of ±1.5%. Comparison between the measured and estimated rotor position is plotted along with the stator current to show an efficient angle tracking mechanism of the proposed method.

Case (ii) An angular rotor speed and position tracking ability under low speed operating region of the generator is tested with the proposed method. Initially, the machine is operated closely to 50% of the generator rated speed i.e. 159 rad/s and at time t = 10 s the speed is changed nearly to 25% (77.19 rad/s). The performance comparison of the measured and estimated angular frequency is depicted in Fig.7(a). Also, the rotor position comparison between the actual and estimated value with the corresponding variation in stator current is shown in Fig.7(b).

Case (iii) The rotor speed and position tracking ability of the proposed method with inverter non-linearities is analysed in this case. It is observed from Fig.8(a) and (c) that considerable percentage of oscillation appears in the d-q stator flux components prior to the filtering stage. However, with the proposed method the oscillation in the flux components is completely suppressed as indicated in Fig(b) and (d), and the precise rotor speed and position estimation is illustrated in Fig.8(e) and (f), respectively.

Case (iv) The measured and the estimated rotor position during the grid disturbance of 70% voltage dip and +10° phase jump in 'a-phase' grid voltage is shown in Fig. 9. The fault is created at t = 5 s and cleared at t = 8 s. The ripple exists in the estimated d-q components of the stator flux due to the presence of twice the grid frequency oscillations in the dc-link voltage and grid active power as depicted in Fig. 9(h) and (i) during the grid fault condition. How-

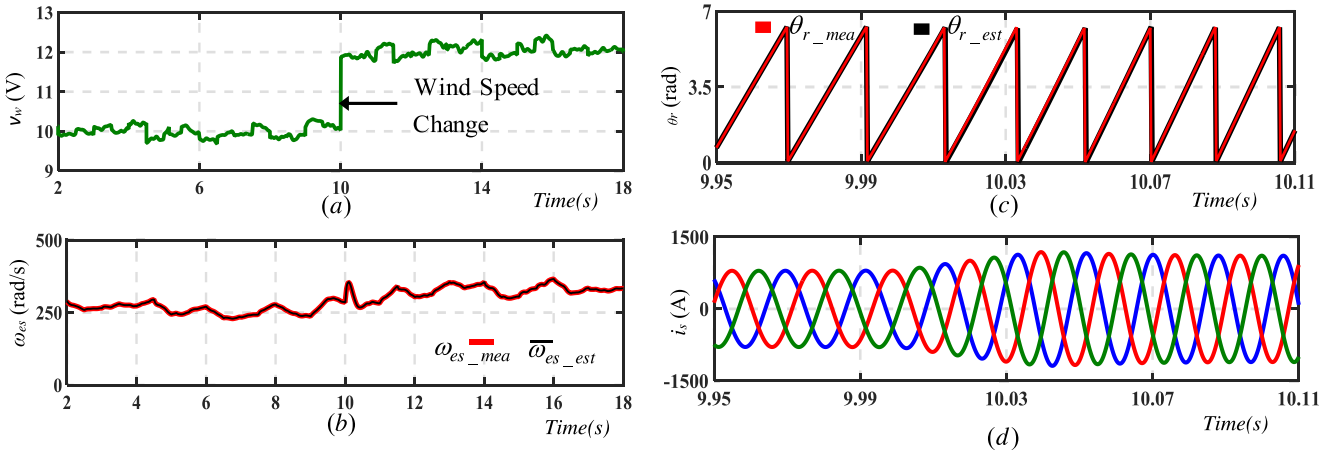

Fig. 6. Rotor angular frequency and position computation for the change in wind speed (a) wind profile, m/s; (b) measured and estimated rotor angular frequency, rad/s; (c) measured and estimated rotor position, rad; (d) three-phase stator current, A.

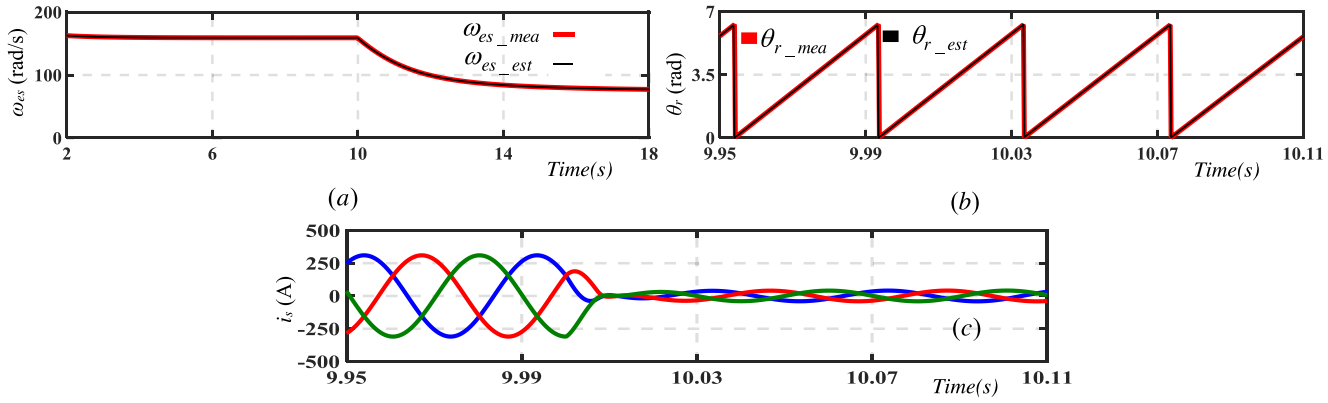

Fig. 7. Rotor angular frequency and position computation for lower speed region: (a) measured and computed rotor angular frequency, rad/s; (b) measured and computed rotor position, rad; (c) stator current, A.

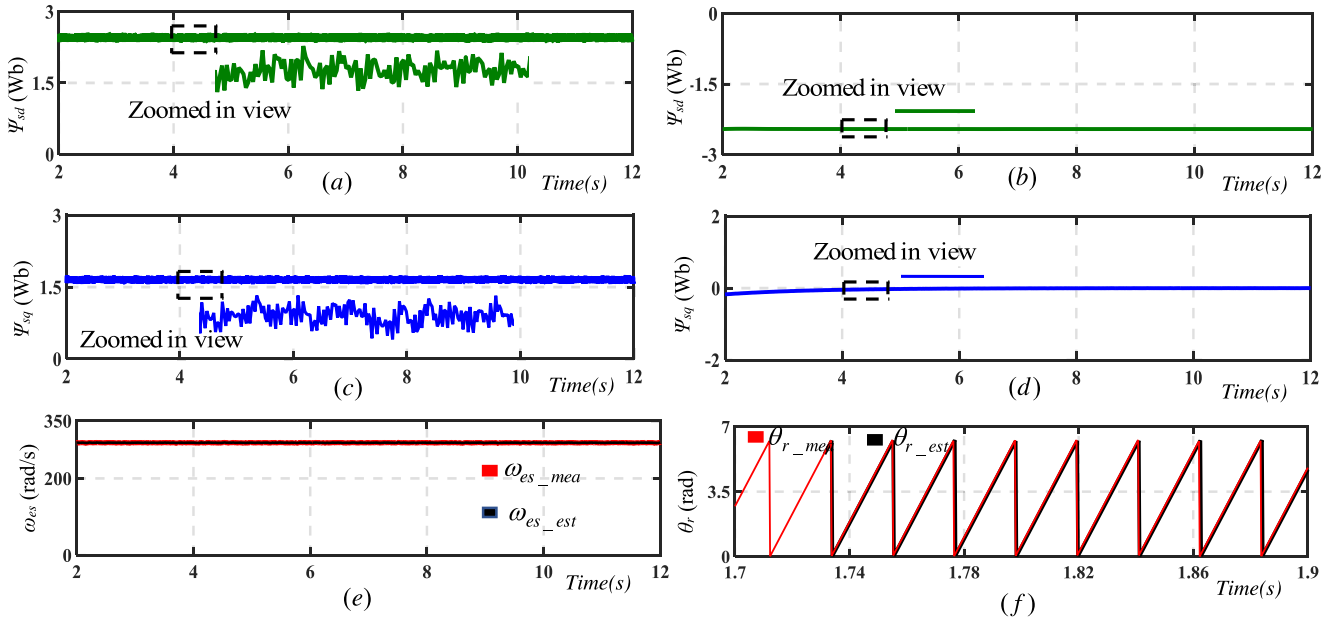

Fig. 8. Rotor angular frequency and position computation under the effect of inverter non-linearities: (a), (b) stator d flux components before pre-stage filter and after PLL synchronization, Wb; (c), (d) stator q flux components before pre-stage filter and after PLL synchronization, Wb; (e) measured and computed rotor angular frequency, rad/s; (f) measured and computed rotor position, rad.

ever, due to the incorporation of a pre-stage LPFs the ripple in the components are filtered out and the rotor position is estimated exactly. During grid disturbance, the active power reference P_g^* on the GSC is regulated with respect to the reduction in grid voltage and generator rated speed. P_g^* is initially set to 1.46 MW to capture the maximum power from the WTG and later it is reduced to 1.39 MW corresponds to rated speed of the generator. This change in power regulation causes the generator speed to change from 322.06 rad/s to 368.55 rad/s and their respective estimated rotor positions under transient period is depicted in Fig. 9(f) and (g). Fig. 9(j) and (k) compares the grid current waveform shape between the conventional and proposed GSC vector control schemes during fault period.

Case (v) Rotor position estimation under the distorted utility condition with 7% of 5^{th} and 7^{th} harmonic components are depicted in Fig. 10. The distorted condition is created at t = 5 s and cleared at t = 8 s. Since there is no reduction in grid voltage, the active power reference $P_g^* = 1.46MW$ is maintained during disturbance period also. The frequency of oscillation in the grid active power during the distorted period is six times the grid frequency as presented in Fig. 10(d). During this period, the percentage of error between the measured and computed angular frequency falls within 0.05%. The proposed GSC controller gives sinusoidal and symmetrical grid current pattern even under distorted utility compared to conventional controller as shown in Fig. 10(e) and (f).

6. Conclusion

A direct method of an angular reference speed is initially computed based on the stator EMF to update the speed tracking mechanism of the PLL. Contradictory to the conventional way of PLL rotor position estimation, the SRF PLL is implemented primarily to determine the assigned stator flux position and then the rotor position is computed using this stator flux position. The major advantage of this proposed method is that observer based model is not required with complex controller design to estimate the system quantities. Also, this method results in fast-dynamic response due to pre-filtering and frequency updating stages. The effective-

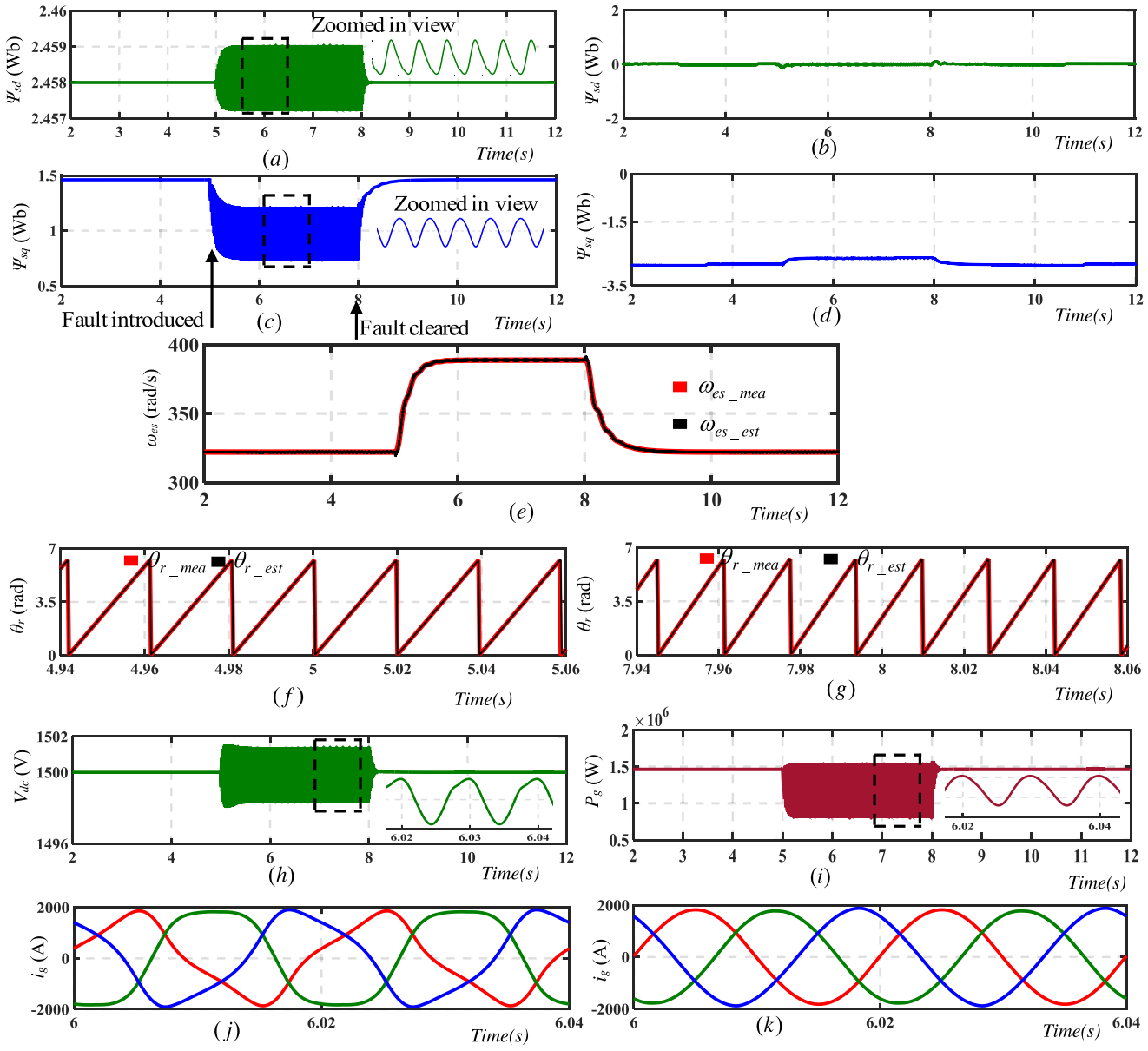

Fig. 9. Rotor speed and position computation under a grid disturbance of 70% voltage sag and +10° phase jump in 'a-phase' (a), (b) stator d flux components before pre-stage filter and after PLL synchronization, Wb; (c), (d) stator q flux components before pre-stage filter and after PLL synchronization, Wb; (e) measured and computed rotor angular frequency, rad/s; (f), (g) estimated and measured rotor position during transient, rad; (h) dc-link voltage, V; (i) grid active power, W; (j), (k) grid current under grid disturbance with conventional and proposed GSC controller, A.

ness of the proposed method is validated by adopting the sensorless vector control of grid tied PMSM based WG under various dynamic operating conditions such as wind speed variation and grid disturbances.

Accurate rotor position estimation, with a steady state and transient error of less than +0.2° and +1° under speed transitions, and low settling time validates the proposed scheme. Equally, the worst case steady state and transient error in speed estimation is less than 0.2% and 1.5% respectively under various grid disturbances. Furthermore, the scheme possesses high starting position tracking ability with reduced steady state and transient errors under various dynamic operating conditions.

Appendix A

Multiple-pole PMSM parameters

Power	P_m	1.5 MW
Speed	ω_m	28 r/min
Current	I_s	961.5 A
Torque	T_L	5.7×10^5 N-m
Number of pole pairs	p_p	120
Armature resistance	R_s	0.0081 Ω
Magnet flux linkage/pole	Ψ_{PM}	2.458 Wb
d-q axis inductance	L_{sd}=L_{sq}	1.2 mH

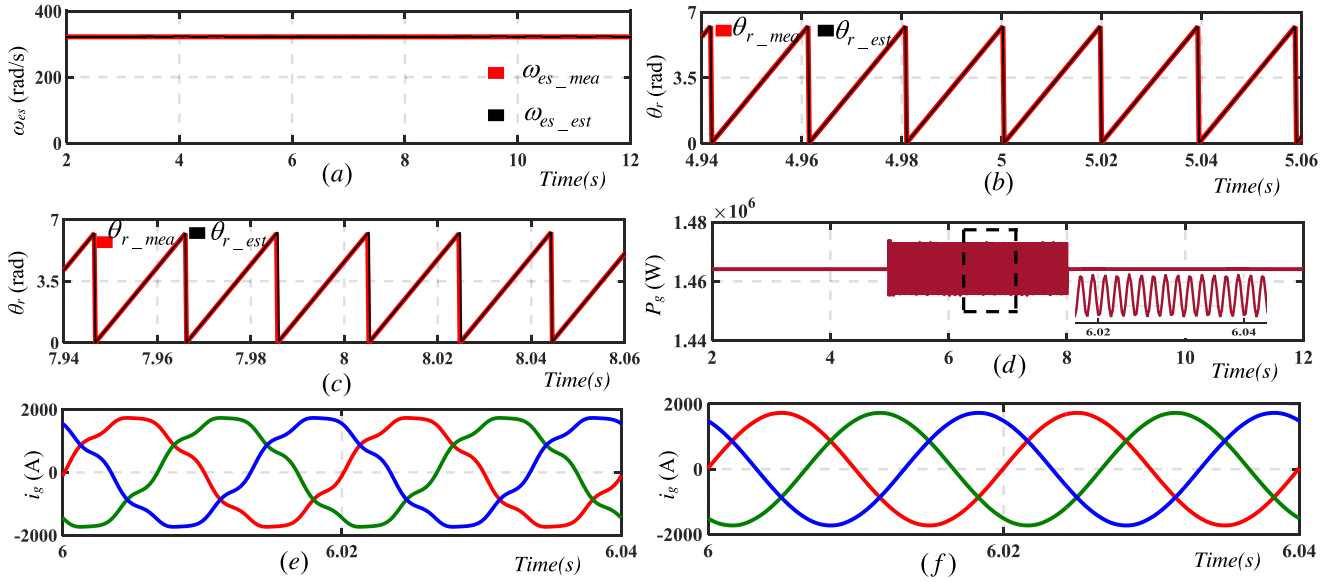

Fig. 10. Rotor angular frequency and position computation under distorted utility condition: (a) measured and computed rotor angular frequency, rad/s; (b), (c) measured and computed rotor position during transient, rad; (d) grid active power, W; (e), (f) grid current under distorted utility condition with conventional and proposed GSC controller, A.

Appendix B

Nomenclature

v, i	Instantaneous value of voltage and current
e, ψ	Instantaneous value of EMF and flux
T_{wt}, T_{sh}	Wind turbine and shaft mechanical torque
T_e	Electromagnetic torque of PMSM
ω_{es}	Angular velocity of PMSM
$J_{wt} and J_r$	Moment of Inertia of wind turbine and PMSM
R_s, L_s	Stator resistance and inductance of PMSM
ψ_{PM}	PMSM rotor flux
p_p	Number of pole pairs
dcandosc	dc and oscillating components.
θ_r	Angle between β-axis and rotor d-axis
δ	Angle between β-axis and assigned d_a-axis
First subscript	
s, r	Stator and rotor
d, q	Synchronous reference frame
α, β	Stationary reference frame

References

[1] Veysel T. Buyukdegirmenci, Ali M. Bazzi, Philip T. Krein, Evaluation of induction and permanent-magnet synchronous machines using drive-cycle energy and loss minimization in traction applications, IEEE Trans. Indus. App. 50 (1) (Jan. 2014) 395–403.

[2] Jonathan Michael Crider, Scott D. Sudhoff, An inner rotor flux-modulated permanent magnet synchronous machine for low-speed high-torque applications, IEEE Trans. Energy Convers. 30 (3) (Sept. 2015) 1247–1254.

[3] Shigeo Morimoto, Trend of permanent magnet synchronous machines, IEEJ Trans. Electr. Electron. Eng. 2 (2007) 101–108.

[4] H. Li, Z. Chen, Overview of different wind generator systems and their comparisons, IET Renew. Power Gener. 2 (2) (2008) 123–138.

[5] Anissia Beainy, Chantal Maatouk, Nazih Moubayed, Fouad Kaddah, Comparison of different types of generator for wind energy conversion system topologies, 3rd International Conference on Renewable Energies for Developing Countries (REDEC), 2016.

[6] M. Tripathi, A.N. Tiwari, Deependra Singh, Grid-integrated permanent magnet synchronous generator based wind energy conversion systems: a technology review, Renewable Sustainable Energy Rev. 51 (2015) 1288–1305.

[7] Y. Park, S. Sul, Implementation schemes to compensate for inverter nonlinearity based on trapezoidal voltage, IEEE Trans. Ind. Appl. 50 (2) (2014) 1066–1073.

[8] D. Park, K. Kim, Parameter-independent online compensation scheme for dead time and inverter nonlinearity in IPMSM drive through waveform analysis, IEEE Trans. Ind. Electron. 61 (2) (Feb. 2014) 701–707.

[9] Lei Yuan, Fei Xiao, Jian-qing Shen, Ming-liang Chen, Qiao-ming Shi, Li Quan-feng, Sensorless control of high-power interior permanent magnet synchronous motor drives at very low speed, IET Electr. Power Appl. 7 (3) (2013) 199–206.

[10] Yue Zhao, Chun Wei, Zhe Zhang, Wei Qiao, A review on position/speed sensorless control for permanent-magnet synchronous machine-based wind energy conversion systems, IEEE Trans, Power Electron. 1 (4) (2013) 203–215.

[11] Mukhtiar Singh, Ambrish Chandra, Application of adaptive network-based fuzzy inference system for sensorless control of pmsg-based wind turbine with nonlinear-load-compensation capabilities, IEEE Trans. Power Electron 26 (1) (Jan 2011) 165–175.

[12] Mahdi Zolfaghari, Seyed Abbas Taher, David Vindel Munuz, Neural network-based sensorless direct power control of permanent magnet synchronous motor, Ain Shams Eng. J. 7 (2016) 729–740.

[13] Tomonobu Senjyua, Satoshi Tamakia, Endusa Muhandoa, Naomitsu Urasakia, Hiroshi Kinjoa, Toshihisa Funabashib, Hideki Fujitac, Hideomi Sekine, Wind velocity and rotor position Sensorless maximum power point tracking control for wind generation system", Renewable Energy 31 (2006) 1764–1775.

[14] Hyun Lee, Jangmyung Lee, Design of iterative sliding mode observer for sensorless PMSM control, IEEE Trans. Control Systems Tech. 21 (4) (July 2013) 1394–1399.

[15] Zhaowei Qiao, Tingna Shi, Yindong Wang, Yan Yan, Changliang Xia, Xiangning He, New sliding-mode observer for position sensorless control of permanent-magnet synchronous motor, IEEE Trans. Indus. Electron. 60 (2) (Feb. 2013) 710–719.

[16] Yue Zhao, Wei Qiao, Wu. Long, An adaptive quasi-sliding-mode rotor position observer-based sensorless control for interior" permanent magnet synchronous machines, IEEE Trans. Power Electron. 28 (12) (Dec. 2013) 5618–5629.

[17] M. Enamul Haque, Y.C. Saw, Mujaddid Morshed Chowdhury, Advanced control scheme for an ipm synchronous generator-based gearless variable speed wind turbine, IEEE Trans Sust. Energy 5 (2) (April 2014) 354–362.

[18] Dirk Paulus, Jean-François Stumper, Ralph Kennel, sensorless control of synchronous machines based on direct speed and position estimation in polar stator-current coordinates, IEEE Trans. Power Electron. 28 (5) (May 2013) 2503–2513.

[19] Zhe Zhang, Yue Zhao, Wei Qiao, Qu. Liyan, A Space-vector-modulated sensorless direct-torque control for direct-drive PMSG wind turbines, IEEE Trans. Indus. Appl. 50 (4) (2014) 2331–2341.

[20] Yuchao Shi, Kai Sun, Lipei Huang, Yongdong Li, Online identification of permanent magnet flux based on extended kalman filter for IPMSM drive with position sensorless control, IEEE Trans. Indus. Electron. 59 (11) (2012) 4169–4178.

[21] Yue Zhao, Wei Qiao, Wu. Long, Improved rotor position and speed estimators for sensorless control of interior permanent-magnet synchronous machines, IEEE Trans. Power Electron. 2 (3) (Sep. 2014) 627–639.

[22] Xu. Wei Qiao, Xiang Gong Yang, Wind speed and rotor position sensorless control for direct-drive PMG wind turbines, IEEE Trans. Indus. App. 48 (1) (Jan 2012) 3–11.
[23] Jianhu Yan, Heyun Lin, Yi Feng, Xun Guo, Yunkai Huang, Z.Q. Zhu, Improved sliding mode model reference adaptive system speed observer for fuzzy control of direct-drive permanent magnet synchronous generator wind power generation system, IET Renew. Power Gener 7 (1) (2013) 28–35.
[24] Suman Maiti, Chandan Chakraborty, Sabyasachi Sengupta, Simulation studies on model reference adaptive controller based speed estimation technique for the vector controlled permanent magnet synchronous motor drive, Simul. Modelling Practice Theory 17 (2009) 585–596.
[25] Xinda Song, Jiancheng Fang, Bangcheng Han, Shiqiang Zheng, Adaptive compensation method for high-speed surface PMSM sensorless drives of EMF-based position estimation error, IEEE Trans. Power Electron. 31 (2) (Feb. 2016) 1438–1448.
[26] Guoqiang Zhang, Gaolin Wang, Xu. Dianguo, Nannan Zhao, ADALINE-network-based PLL for position sensorless interior permanent magnet synchronous motor drives, IEEE Trans. Power Electron. 31 (2) (Feb. 2016) 1450–1460.
[27] Silverio Bolognani, Sandro Calligaro, Roberto Petrella, Design issues and estimation errors analysis of back-EMF-based position and speed observer for SPM synchronous motors, IEEE Power Electron. 2 (2) (June 2014) 159–170.
[28] Jin-Sik Park, Shin-Myung Jung, Hag-Wone Kim, Myung-Joong Youn, Design and analysis of position tracking observer based on instantaneous power for sensorless drive of permanent magnet synchronous motor, IEEE Trans. Power Electron. 27 (5) (May 2012) 2585–2594.
[29] Li Tong, Xudong Zou, Yu. ShuShuai Feng, Yong Kang Chen, Qingjun Huang, Yanrun Huang, An SRF-PLL-based sensorless vector control using the predictive deadbeat algorithm for the direct-driven permanent magnet synchronous generator, IEEE Trans. Power Electron. 29 (6) (June 2014) 2837–2849.
[30] Chih-Ming Hong, Chiung-Hsing Chen, Tu. Chia-Sheng, Maximum power point tracking-based control algorithm for PMSG wind generation system without mechanical sensors, Energy Conver. Manage. 69 (2013) 58–67.
[31] Sami Zaim, Babak Nahid-Mobarakeh, Farid Meibody-Tabar, Robust position sensorless control of nonsalient pmsm at standstill and low speeds, IEEE Trans. Power Electron. 2 (3) (Sept. 2014) 640–650.
[32] I. Boldea, The Electric Generators Handbook: Variable Speed Generators, CRC Press, 2006.
[33] S.M. Muyeen, M.H. Ali, R. Takahashi, T. Murata, J. Tamura, Y. Tomaki, A. Sakahara, E. Sasano, Comparative study on transient stability analysis of wind turbine generator system using different drive train models, IET Renew. Power Gener. 1 (2) (Jun. 2007) 131–141.
[34] M.A. Asha Rani, C. Nagamani, G. Saravana Ilango, An improved rotor PLL(R-PLL) for enhanced operation of doubly fed induction machine, IEEE Trans. Sust Energy. 8 (1) (Jan. 2017) 117–125.
[35] O. Alizadeh, A. Yazdani, A strategy for real power control in a direct-drive PMSG-based wind energy conversion system, IEEE Trans. Power Delivery 28 (3) (July 2013) 1297–1305.
[36] K.-H. Kim, Y.-C. Jeung, D.-C. Lee, LVRT scheme of PMSG wind power systems based on feedback linearization, IEEE Trans. Power Electron. 27 (5) (May 2012) 2376–2384.
[37] H. Geng, G. Yang, D. Xu, B. Wu, Unified power control for PMSG-based WECS operating under different grid conditions, IEEE Trans. Energy Convers. 26 (3) (Sep. 2011) 822–830.
[38] Eider Robles, Salvador Ceballos, Josep Pou, et al., Variable-frequency grid-sequence detector based on a quasi-ideal low-pass filter stage and a phase-locked loop, IEEE Trans. Power Electron. 25 (10) (2010) 2552–2563.